J Math Chem (2014) 52:1563–1575
DOI 10.1007/s10910-014-0336-y

ORIGINAL PAPER

Informational thermodynamic model for nanostructures

Forrest H. Kaatz · Adhemar Bultheel

Received: 24 January 2014 / Accepted: 5 February 2014 / Published online: 20 February 2014

Abstract Nanostructures may be fabricated from metal nanoclusters such as gold or platinum, which are of interest for catalytic and structural characteristics, or from nano forms of carbon allotropes. Here, informational thermodynamic properties such as free energy, enthalpy, and entropy are calculated using a graph network model at T = 298.15 K. We calculate the partition function using Euclidean adjacency matrices from the Hamiltonian and estimated bond energies. The summed atomic displacement from the Kirchhoff index has power law behavior, while the thermodynamic properties exhibit large N logarithmic behavior: however, the data shows structurally related anomalies.

Keywords Metal nanocluster · Statistical thermodynamics · Nano carbon

1 Introduction

1.1 Metal nanoclusters

Gold and platinum have been valued for ornamental jewelry since antiquity. In particular, pure gold does not easily bond with other elements and is known as the 'noblest' of metals. In recent years, man has created nano forms of gold and platinum, which have markedly different characteristics than the bulk materials. The nanosized form of gold exhibits catalytic properties unknown in the bulk [1]. Likewise, nanosized platinum has remarkable catalytic properties, with icosahedral platinum clusters recently reporting an area-specific activity of 0.83 mA/cm^2 Pt, in an oxygen reduction reaction (ORR) [2].

F. H. Kaatz (✉)
Mesalands Community College, 911 South 10th Street, Tucumcari, NM 88401, USA
e-mail: fhkaatz@gmail.com

A. Bultheel
Department of Computer Science, KU Leuven, Celestijnenlaan 200A, 3001 Heverlee, Belgium

Table 1 Magic number formulas for the icosahedral, cuboctahedral, and decahedral structures

Definition	Notation	Cluster structure		
		ICO	CO (FCC)	DECA
Total number of atoms	N	$10\frac{L^3}{3}+5L^2+11\frac{L}{3}+1$	$10\frac{L^3}{3}+5L^2+11\frac{L}{3}+1(L \text{ even})$ $10\frac{L^3}{3}+3L^2-\frac{L}{3}(L \text{ odd})$	$5\frac{L^3}{6}+\frac{L}{6}$
Number of surface atoms	N_S	$10L^2+2$	$10L^2+2(L \text{ even})$ $10L^2-4L(L \text{ odd})$	$5L^2-10L+7$
Number of bonds	N_B	$20L^3+12L^2+4L$	$20L^3+15L^2+7L(L \text{ even})$ $20L^3-8L(L \text{ odd})$	$5L^3-15\frac{L^2}{2}+7\frac{L}{2}-1$

The first one has been published in references [3,4], while the cuboctahedral and decahedral ones are new

The phrase 'nanocluster' is often used to describe nanosized metal particles, since they can form structures which strictly speaking are not crystalline in that they do not have bulk symmetry, whereas a cluster sized form may exist in the nano regime. There are many types of shape and symmetry which may exist in nanosized materials [3], among them icosahedral, cuboctahedral, and decahedral. Gold and platinum are face-centered-cubic (FCC) metals, so we use this structure for the nanosized material. Note that the cuboctahedral clusters can be described as an FCC structure, whereas the icosahedral and decahedral cannot. We examine the properties of gold and platinum nanoclusters with these symmetries for sizes up to several thousand atoms.

Nanoclusters are created from atoms completing layers or shells sequentially giving rise to what has been phrased as 'magic numbers', or the number of atoms to complete a shell over a beginning layer. Thus, for some clusters, there has developed a large description of formulas, giving the relation of number of atoms, surface atoms, and bonds as a function of L, the number of shells in the cluster [4]. A summary of these formulas for icosahedral, cuboctahedral, and decahedral clusters for our purposes is given in Table 1. We note that gold nanoclusters have been formed in the icosahedral [5–8], cuboctahedral [9], decahedral [6,8,10], and cubic [5] forms. Also, platinum has been made in the icosahedral [2,11], cuboctahedral [12], decahedral [11], and cubic [12,13] shapes.

There are some previous studies on the thermodynamic properties of gold and platinum nanoclusters. There is a plethora of models regarding the melting of clusters, but not when it comes to describing the thermodynamic properties of gold and platinum nanoclusters specifically. A study of gold nanoclusters [14] looked at the internal energy, entropy, and free energy as a function of cluster size, using molecular dynamics and the 'glue' potential for gold. Also, a molecular dynamics study on platinum nanoclusters [15] showed that the melting temperature, enthalpy, and entropy can be approximated by a linear model of $N^{(-1/3)}$, where N is the number of atoms in the nanocluster.

1.2 Carbon nanostructures

Carbon allotropes exhibit an amazing diversity of structure, properties, and bonding. Carbon nanostructures consist of fullerenes, endohedral fullerenes, nanotubes, and the

related forms of nanobuds, nano-onions, nanotori and graphene nanoflakes [16]. The first fullerene, C_{60}, was discovered in 1985 [17], nanotubes in 1991 [18], and graphene in 2004 [19]. The highly valued allotrope, diamond, is transparent and semiconducting with sp^3 hybrid bonds, while the thermodynamically stable graphite is an opaque conductor with sp^2 bonding. The nanostructures demonstrate an equally diverse character, with a variety of structures and properties.

Bonding in carbon compounds ranges from single C–C bonds to triple C ≡ C bonds with a range of bond energy with the different types of bonds. In 1947, Gordy postulated that the bond energy varies as the inverse square of the bond length, with empirical coefficients [20]. These parameters were updated by Paolini in 1990 [21]. Pauling came up with an inverse variation of bond energy to bond length for carbon compounds in 1954 [22]. The nanostructures, in particular, most frequently have sp^2 hybrid bonding [23]. Previous molecular-dynamics (MD) modeling shows that fullerenes and nanotubes can self-assemble from high temperature amorphous carbon precursors [24,25]. Also, for nanotubes, there are some existing models for arc-evaporated or laser-vaporization processes [25]. However, a thorough understanding needs more work, especially in the case where catalytic particles are not part of the growth model.

It has taken some time after the original discoveries of the carbon nanostructures for their thermal properties to be measured. There exist a few results for C_{60} [26], and nanotubes were only recently measured by a Russian group [27]. These groups measured the specific heat, enthalpy, entropy, and Gibbs free energy for C_{60} and nanotubes, respectively. Our approach consists of an informational complex systems method, based on the statistical mechanics of networks and graph theory [28]. In this approach, atoms are situated at the vertices of the network, and bonds are represented by links between vertices. In this way, we can model the behavior of different systems, but we caution that this is not a molecular dynamics (MD) procedure, or even density functional theory (DFT). Thus our calculations are not directly comparable to the experimental thermal properties measured by other groups.

2 Methods

We use a theoretical graph—network approach, with atoms at the vertices, and links as nearest neighbor bonds. An adjacency matrix is created which contains a 1 at position (i, j) if atom j is in the set of nearest neighbors of atoms i, i.e., when the distance r_{ij} is approximately equal to $r_{\min} = \min_{i \neq j} r_{ij}$. To allow for small deviations from the average bond length, we shall define i and j as nearest neighbors, and separate them from the rest by requiring that $r_{ij} < r_c$ where r_c is a threshold value, appropriate for the nanocluster. Thus,

$$\mathbf{A}(i, j) = \begin{cases} 1 \text{ if } r_{ij} < r_c \text{ and } i \neq j \\ 0 \text{ otherwise.} \end{cases} \tag{1}$$

As an alternative, we may consider the actual Euclidean distances in the adjacency matrix, i.e., replace every nonzero entry $\mathbf{A}(i, j)$ in the previous definition by the actual

Table 2 Experimental parameters for gold, platinum, and carbon

Parameter	Gold	Platinum	Carbon
D_0(eV)	2.302 [29]	3.683 [30]	6.0 [30]
β_r (Å^{-1})	1.586426 [29]	1.64249 [30]	2.1 [30]
S	1.95 [29]	2.24297 [30]	1.22 [30]
r_0 (Å)	2.463316 [29]	2.384 [30]	1.39 [30]
Gx10^{10} (N/m^2) (298 K)	2.60 [33]	6.09 [33]	N/A
γ (J/m^2) (298 K)	2.052 [33]	2.502 [33]	N/A
r_b (Å) (bulk)	2.884 [34]	2.775 [35]	N/A
k (N/m)	21.7 [39]	48.3 [40]	305 [41] graphene

The source of the reference is listed in brackets

distance r_{ij} and keep the zeros. We use the modified Euclidean matrix to create a model Hamiltonian.

Recently, the Pauling relation gives the bond energy as a function of bond distance as

$$E_B = D_0 \exp\left[-\beta_r \sqrt{2S}(r_b - r_0)\right] \tag{2}$$

where r_b is the nearest neighbor bond length, in angstroms and the other parameters are empirically derived [29,30]. See Table 2 for a list of parameters for gold, platinum, and carbon. We then use a nearest neighbor Hamiltonian, $H = E_B$ in the calculations. It is worth mentioning that the nearest neighbor distances in icosahedra do not consist of a single bond length, but that these structures have two neighboring distances, with the tangential bond length to radial bond length ratio given by

$$\frac{r_{\tan}}{r_{rad}} = \frac{2}{(5)^{1/4}\sqrt{\tau}} \approx 1.05; \tau = \frac{(1+\sqrt{5})}{2} \tag{3}$$

and τ is the golden mean [31]. Also, carbon nanostructures may have bonds of differing lengths as fullerenes are known to have several nearest neighbor bonds [32]. Our Hamiltonian accounts for these changes in bond length in a well-defined manner, through the variation of E_B.

It has been observed that the lattice constant of metal nanoclusters decreases from the bulk value as the size of the cluster becomes smaller. A model for this behavior is given by

$$\frac{\Delta a}{a} = -\frac{1}{1 + K \cdot D}; \; K = \frac{\alpha^{1/2} G}{\gamma} \tag{4}$$

where a is the lattice constant, G is the shear modulus, γ is the surface energy, α is a shape factor (=1 for a spherical particle) and D (= 2R) is the nanocluster diameter in angstroms [33]. The relevant values for these parameters are listed in Table 2. Experimentally, this behavior is confirmed, with measurements for both gold [34], and platinum [35]. The nearest neighbors in the [110] direction determine the bond length in an FCC metal with $r_b = \sqrt{2}a/2$. Originally, the complex systems network theory used the adjacency matrix [28] in the model, but we use the more general

Hamiltonian approach, where the partition function is

$$Z = \mathrm{Tr}\, e^{-\beta \mathbf{H}} \tag{5}$$

and $\beta = 1/k_B T$ is the inverse temperature, with k_B Boltzmann's constant, T = 298.15 K or room temperature for our purposes, and **H** is the Hamiltonian matrix. We calculate the Euclidean adjacency matrix and use E_B to convert it into the Hamiltonian. The statistical mechanics quantities are then calculated from the probability of occupying a state j as

$$p_j = \frac{e^{\beta \lambda_j}}{Z} \tag{6}$$

where λ_j is an eigenvalue of the Hamiltonian matrix. The informational Shannon entropy is then

$$S(G, \beta) = -\sum_{j=1}^{N} p_j \ln p_j \tag{7}$$

for a graph G [37]. The total energy H, or enthalpy, and Helmholtz free energy, F, are related by $F = H–TS$, which results in the expressions

$$H(G, \beta) = -\frac{1}{Z} \mathrm{Tr}\left(-\mathbf{H} e^{-\beta \mathbf{H}}\right) \tag{8}$$

and

$$F(G, \beta) = -\frac{1}{\beta} \ln Z \tag{9}$$

where **H** is again the Hamiltonian matrix [28]. As written, the entropy is dimensionless, while the enthalpy has units of E_B, and the free energy has units related to $k_B T$. However, since we are not comparing our results to experimentally measured data, we do not try to interpret the results with more than the N dependence growth.

The summed atomic displacement may be calculated from Kirchhoff index, and is valid for any graph G [37]. The Kirchhoff index can be determined from the Laplacian matrix, where **L** is defined as

$$\mathbf{L} = \Delta - \mathbf{A} \tag{10}$$

and Δ is a diagonal matrix of order N, with diagonal elements = the number of first neighbors, or the number of non-zero entries in a column in the adjacency (0,1) matrix, **A** [38]. Then the Kirchhoff index is

$$Kf(G) = N \sum_{i=1}^{N-1} \frac{1}{\lambda_i} \tag{11}$$

and λ_i is an eigenvalue of **L,** with the Nth eigenvalue omitted since it equals zero [38]. The atomic displacement is given as

$$\Delta x = \sqrt{\sum\nolimits_{i=1}^{N} (\Delta x_i)^2} = \sqrt{\frac{1}{\beta k N} Kf(G)} \tag{12}$$

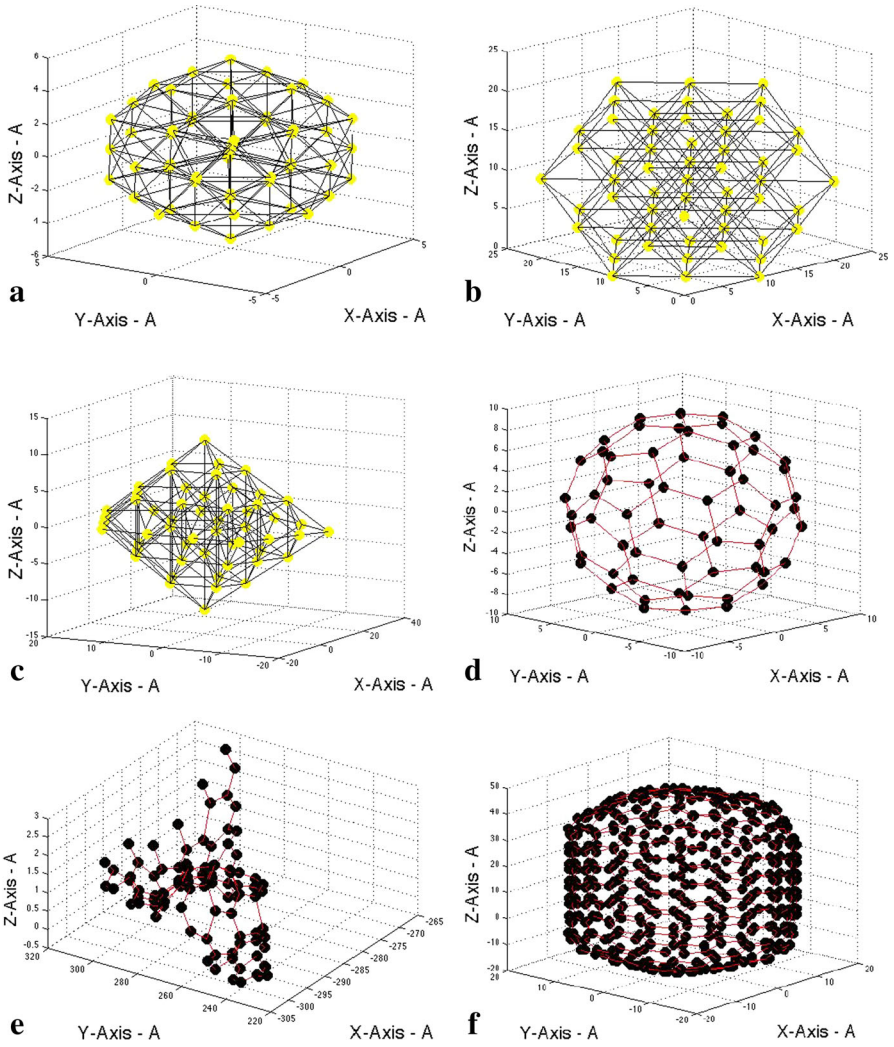

Fig. 1 Nanostructures examined in this manuscript. **a** Icosahedron 55 atoms. **b** Cuboctahedron 55 atoms. **c** Decahedron 54 atoms **d** Carbon C_{60}. **e** 100 atom graphene nanoflake. **f** (10,10) nanotube

where k is the material nearest neighbor force constant, and β is the inverse temperature [37]. We use the bulk force constant for gold [39] platinum [40] and carbon (graphene) [41], since clusters over 13 atoms have this larger value [39].

3 Results

We plot the nanostructures we examine in Fig. 1, including clusters of icosahedra, cuboctahedra, and decahedra, as well as nano forms of carbon: C_{60}, graphene nanoflakes, and a (10,10) nanotube. The results of the thermodynamic calculations

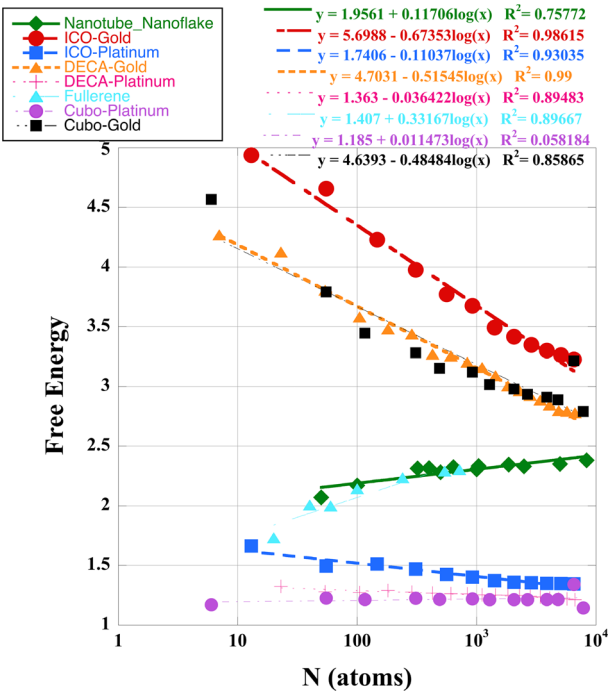

Fig. 2 Free energy of the nanostructures versus N, the number of atoms

are plotted in Figs. 2, 3, and 4. These three figures show the thermodynamic properties of fullerenes from C_{20} to C_{720}, graphene nanoflakes up to 5,000 atoms in size, and of a nanotube, the (10,10) armchair version, with up to 8,360 atoms. Figure 2 shows the plots of free energy, F, as a function of N, while Figs. 3 and 4 show the enthalpy, H, and entropy, S, respectively. In Figs. 2 and 3, the free energy and enthalpy fits have opposite slopes in the data presented. The negative slope is directly related to the decreasing bond length of the metal nanoclusters and the bond energy while the carbon forms show a positive slope since the bond length is unrelated to N. The least-squares regression for the fit, R^2, is shown in the inset.

The entropy calculations in Fig. 4 show anomalies for the fullerenes, icosahedral, and cuboctahedral structures. The fullerene and icosahedral curves have an anomaly at $N = 55$–60, while the cuboctahedral structure has a dip at $N = 6{,}525$. It is known that the fullerene C_{60} has different bond lengths ranging from 1.455 Å to 1.391 Å [42]. The small values are very close the value of r_0 in Table 2 for carbon. Such a wide variation does not occur in neighboring fullerenes [32]. Table 3 shows the nearest neighbor count for the icosahedral and cuboctahedral structures near the entropy anomalies. For the icosahedral 55 atom structure, there are zero 9-coordinated neighbors, while the cuboctahedral 6,525 atom structure has zero 7-coordinated neighbors. This also accounts for the slight increase in the free energy and enthalpy data for the cuboctahedral curves. The decahedral structure does not have any nearest neighbor anomalies, and we see that the corresponding data is smooth. The nearest neighbors

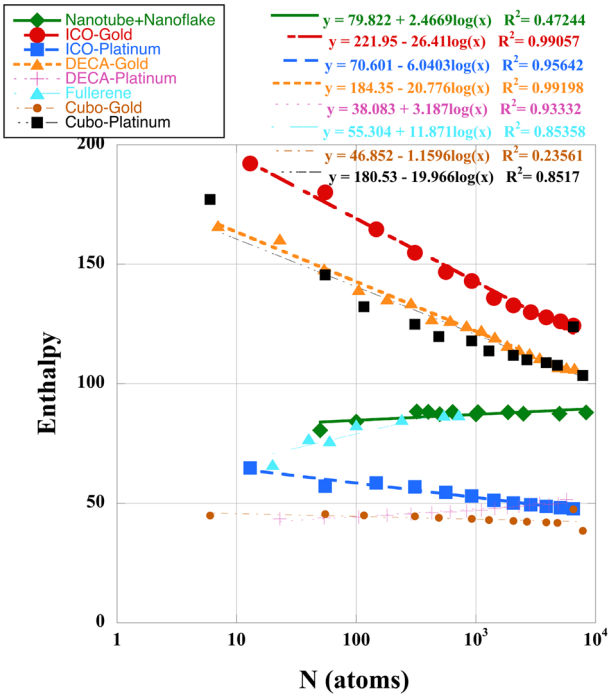

Fig. 3 Enthalpy of the nanostructures versus N, the number of atoms

appear as entries in a column of the Hamiltonian matrix, and thus the eigenvalues are changed affecting the entropy calculations. There is an additional anomaly in that the entropy of the fullerenes does not approach zero as the number of atoms, N, goes to zero. This is no doubt related to the bond length in C_{20}.

Informational entropy has been calculated as far back as 1984 [43] in neutral atoms with Thomas–Fermi statistics. It was postulated then and subsequently in 1998 [36], that informational entropy has logarithmic behavior as a function of N. Massen and Panos [36] modeled the informational entropy for atoms, Na atomic clusters, and nuclei and determined the logarithmic dependence. Estrada and Hatano modeled informational statistical mechanics in 2007 [28], and the large-N behavior was shown to be logarithmic. In all of these modeling situations, the logarithmic dependence arises from the calculations, from the definitions. Based on our data, we suggest that an informational thermodynamic property P, has the following behavior:

$$P = A + B\ln(N) \tag{13}$$

where A and B are universal constants and N is the number of atoms. Note that in Figs. 2, 3 and 4, the fit is better for large N, as suggested by Estrada and Hatano [28]. This generalization does not, however, allow for structural anomalies, which we have shown to affect the data.

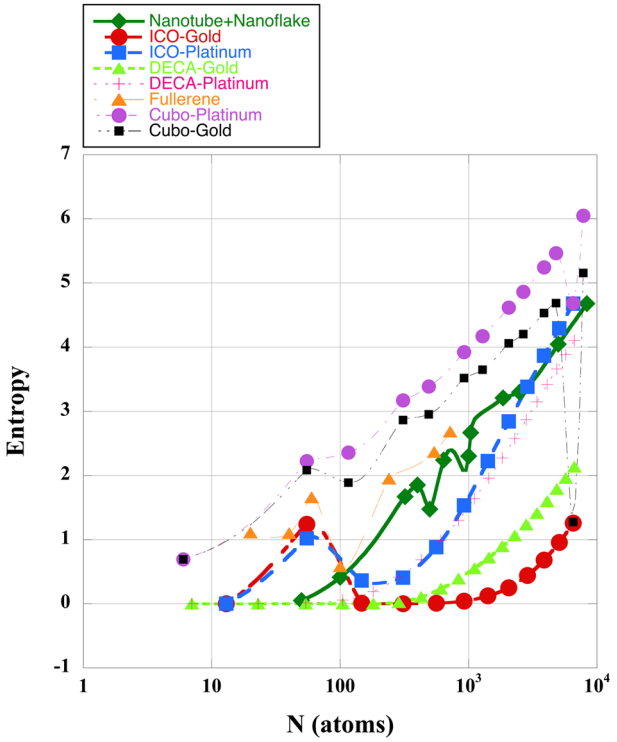

Fig. 4 Entropy of the nanostructures versus N, the number of atoms. The *lines* are smooth curve fits

Table 3 Nearest neighbors counts for icosahedral and cuboctahedral structures

N	N1	N2	N3	N4	N5	N6	N7	N8	N9	N10	N11	N12
I-13	0	0	0	0	0	12	0	0	0	0	0	1
I-55	0	0	0	0	0	12	0	30	0	0	0	13
I-147	0	0	0	0	0	12	0	60	20	0	0	55
CO-4796	0	0	0	0	0	24	216	486	440	0	0	3,630
CO-6525	0	0	0	0	0	12	0	330	1,100	0	0	5,083
CO-7826	0	0	0	0	0	24	264	726	624	0	0	6,188

For example, N6 refers to the number of sites with 6-fold coordinated neighbors. The number of atoms in the structures agrees with the sum of nearest neighbors. Note the differences in the number of neighbors, accounting for the anomalies in the calculations

The atomic displacement is plotted in Fig. 5 for gold and platinum nanoclusters and for carbon nanostructures. These plots follow a power law fit, as might be expected since the Kirchhoff index grows with N, and the major change in the data is the force constant. The Kirchhoff index does not appear to be structurally sensitive.

The growth of carbon nanostructures has not been completely determined. The original fullerene, C_{60}, was formed from cluster beam experiments [17], and a few years later, solid crystals were fabricated, allowing bulk samples to be studied [44].

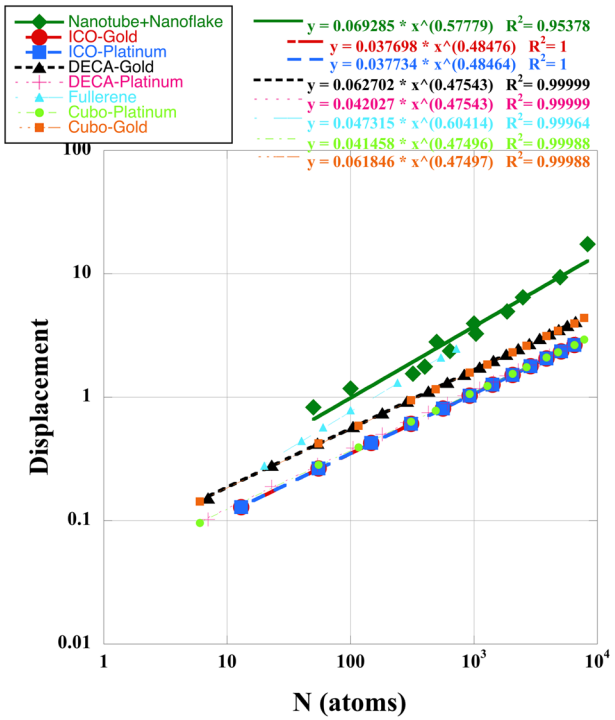

Fig. 5 Atomic displacement of the nanostructures versus N, the number of atoms

Carbon nanotubes are thought to grow from a metal catalyst [45], supplied with a carbon feedstock, with growth terminating at some point. A reliable bottom-up approach to creating graphene nanoflakes has yet to be developed, so that the novel features of these carbon nanostructures remains unexplored. Thus the mechanism of growth as a function of the number of atoms, N, is best determined for carbon nanotubes, with the other structures less well understood.

Likewise, although there has been a large increase in activity of chemical synthesis of metal nanoclusters, so that a large variety of elements, alloys, and structures are now possible, a definitive model for crystal growth is still being developed. Recent progress on gold [46] and platinum [47] nanoclusters includes a nano phase diagram, where the temperature and structure of nanophase material has been plotted. However, platinum especially has been undergoing rapid changes in development, so that additional changes may be expected.

4 Conclusion

We have demonstrated that the informational thermodynamic properties follow a logarithmic relationship for metal nanoclusters and nano forms of carbon. The Hamiltonian was based on nearest neighbor bond energies derived from the Euclidean adjacency matrix. We have accounted for the decreasing size of metal nanoclusters and this affects

the slope of the free energy and enthalpy data. The large N logarithmic behavior is in agreement with preexisting versions of informational statistical mechanics, with the data showing structurally related anomalies. These structural anomalies are related to the variation in nearest neighbor bond length and coordination. The atomic displacement derived from the Kirchhoff index follows a power law regression, increasing with larger numbers of atoms.

Acknowledgments F. H. Kaatz thanks A. Fasolino for sharing atomic coordinates of rippled graphene, and thanks E. Estrada for programming assistance.

5 Appendix

We recently published some results describing power law behavior with the thermodynamic properties [48–50]. We now show that these power law relationships are equivalent to the logarithmic properties shown in this manuscript.

Suppose the thermodynamic property is P and we consider

$$\frac{P}{N_B} = \frac{A + B\ln(N)}{cN} \tag{14}$$

where N_B is the number of bonds and A, B, and c are constants with $N_B = cN$. We then have

$$N = cN - (c-1)N = cN\left(1 - \frac{c-1}{c}\right) \tag{15}$$

and thus

$$\ln(N) = \ln(cN) + \ln\left(1 - \frac{c-1}{c}\right). \tag{16}$$

If we use this expression in Eq. (14), we have

$$\frac{P}{N_B} = \frac{A}{cN} + B\frac{\ln(cN)}{cN} + B\frac{\ln\left(1 + \frac{c-1}{c}\right)}{cN} = \frac{A + B\ln\left(\frac{2c-1}{c}\right)}{cN} + B\frac{\ln(cN)}{cN}. \tag{17}$$

Now both terms on the right go to zero as $N \to \infty$, but the first one is faster than the second one. Hence for large N, the dominant term is $BN_B^{-1}\ln(N_B)$. Because $\ln(N_B) < (N_B)^{\alpha}$ for $N \to \infty$ and $\alpha > 0$, we shall have the result we are intending to prove

$$\frac{P}{N_B} \sim B(N_B)^{-1+\alpha}, N \to \infty, \alpha > 0, \tag{18}$$

and the original expression for P (Eq. 14) shows the logarithmic behavior.

References

1. J. Gong, Chem. Rev. **112**, 2987–3054 (2012)
2. W. Zhou, J. Wu, H. Yang, Nano. Lett. **13**, 2870–2874 (2013)
3. B.K. Teo, N.J.A. Sloane, Inorg. Chem. **24**, 4545–4558 (1985)
4. J.M. Montejano-Carrizales, F. Aguilera-Granja, J.L. Moran-Lopez, NanoStructured Mater. **8**(3), 269–287 (1997)
5. F. Kim, S. Connor, H. Song, T. Kuykendall, P. Yang, Angew. Chem. **116**, 3673–3677 (2004)
6. K. Koga, T. Ikeshoji, K. Sugawara, Phys. Rev. Lett. **92**(11), 15507 (2004)
7. S.W. Lu, V. Frain, M. Arbab, J. Phys. Chem. C **114**, 12850–12854 (2010)
8. K. Koga, K. Sugawara, Surf. Sci. **529**, 23–35 (2003)
9. Y. Li et al., J. Am. Chem. Soc. **134**, 17997–18003 (2012)
10. A. Sanchez-Iglesias, I. Pastoriza-Santos, J. Perez-Juste, B. Rodriguez-Gonzalez, F. Javier, F.J. Garcia de Abajo, L.M. Liz-Marzan, Adv. Mater. **18**, 2529–2534 (2006)
11. W. Zhu, A.-X. Yin, Y.-W. Zhang, C.-H. Yan, Chem. Eur. J. **18**, 12222–12226 (2012)
12. K.M. Bratlie, H. Lee, K. Komvopoulos, P. Yang, G.A. Somorjai, Nano Lett. **7**(10), 3097–3101 (2007)
13. C.M. Sanchez-Sanchez, J. Solla-Gullon, F.J. Vidal-Iglesias, A. Aldaz, V. Montiel, E. Herrero, J. Am. Chem. Soc. **132**, 5622–5624 (2010)
14. Y.H. Chui, G. Grochola, I.K. Snook, S.P. Russo, Phys. Rev. B **75**, 033404 (2007)
15. H. Akbarzadeh, G.A. Parsafar, Fluid Phase Equilib. **280**, 16–21 (2009)
16. J.L. Delgado, M.A. Herranz, N. Martin, J. Mater. Chem. **18**, 1417–1426 (2008)
17. H.W. Kroto, J.R. Heath, S.C. O'Brien, R.F. Curl, R.E. Smalley, Nature **318**, 162–163 (1985)
18. S. Iijima, Nature **354**, 56–58 (1991)
19. K.S. Novoselov, A.K. Geim, S.V. Morozov, D. Jiang, Y. Zhang, S.V. Dubonos, I.V. Grigorieva, A.A. Firsov, Science **306**, 666–669 (2004)
20. W. Gordy, J. Chem. Phys. **15**(5), 305–310 (1947)
21. J.P. Paolini, J. Comput. Chem. **11**(10), 1160–1163 (1990)
22. L. Pauling, J. Phys. Chem. **58**(8), 662–666 (1954)
23. R.C. Powles, N.A. Marks, D.W.M. Lau, Phys. Rev. B **79**, 075430 (2009)
24. Y. Yamaguchi, L. Colombo, P. Piseri, L. Ravagnan, P. Milani, Phys. Rev. B **76**, 134119 (2007)
25. P.J.F. Harris, Carbon **45**, 229–239 (2007)
26. B.V. Lebedev, K.B. Zhogova, T.A. Bykova, B.S. Kaverin, V.L. Karnatsevich, M.A. Lopatin, Russ. Chem. Bull. **45**(9), 2113–2117 (1996)
27. V.B. Muratov, O.O. Vasil'ev, L.M. Kulikov, V.V. Garbuz, Yu.V. Nesterenko, T.I. Duda, J. Superhard Mater. **34**(3), 173–178 (2012)
28. E. Estrada, N. Hatano, Chem. Phys. Lett. **439**, 247–251 (2007)
29. M. Backman, N. Juslin, K. Nordlund, Eur. Phys. J. B **85**, 317–322 (2012)
30. K. Albe, K. Nordlund, R.S. Averback, Phys. Rev. B **65**, 195124 (2002)
31. J.E. Hearn, R.L. Johnston, J. Chem Phys. **107**, 4674–4687 (1997)
32. M. Alcami, G. Sanchez, S. Diaz-Tendero, Y. Wang, F. Martin, J. Nanosci. Nantechnol. **7**, 1329–1338 (2007)
33. W.H. Qi, M.P. Wang, J. Nanoparticle Res. **7**, 51–57 (2005)
34. J.T. Miller, A.J. Kropf, Y. Zha, J.R. Regalbuto, L. Delannoy, C. Louis, E. Bus, J.A. von Bokhoven, J. Catal. **240**, 222–234 (2006)
35. M. Klimenkov, S. Nepijko, H. Kuhlenbeck, M. Baumer, R. Schlogl, H.-J. Freund, Surf. Sci. **391**, 27–36 (1997)
36. S.E. Massen, C.P. Panos, Phys. Lett. A **26**, 530–533 (1998)
37. E. Estrada, N. Hatano, Chem. Phys. Lett. **486**, 166–170 (2010)
38. I. Gutman, B. Mohar, J. Chem. Inf. Comput. Sci. **36**, 982–985 (1996)
39. J.R. Lombardi, B. Davis, Chem. Rev. **102**, 2431–2460 (2002)
40. K. Kern, R. David, R.L. Palmer, G. Comsa, T.S. Rahman, Phys. Rev. B **33**(6), 4334–4337 (1986)
41. S.Y. Davydov, Phys. Solid State **52**, 1947–1951 (2010)
42. W.I.F. David, R.M. Ibberson, J.C. Mathewman, K. Prassides, T.J.S. Dennis, J.P. Hare, H.W. Kroto, R. Taylor, D.R.W. Walton, Nature **353**, 147–149 (1991)
43. S.R. Gadre, Phys. Rev. A **30**(1), 620–621 (1984)
44. W. Kratschmer, L.D. Lamb, K. Fostiropoulos, D.R. Huffman, Nature **347**, 354–358 (1990)

45. F.H. Kaatz, M.P. Siegal, D.L. Overmyer, P.P. Provencio, D.R. Tallant, Appl. Phys. Lett. **89**, 241915 (2006)
46. A.S. Barnard, N.P. Young, A.I. Kirkland, M.A. van Huls, H. Xu, ACS Nano **3**(6), 1431–1436 (2009)
47. A.S. Barnard, H. Konishi, H.F. Xu, Catal. Sci. Technol. **1**, 1440–1448 (2011)
48. F.H. Kaatz, A. Bultheel, J. Math. Chem. **51**, 1211–1220 (2013)
49. F.H. Kaatz, A. Bultheel, J. Math. Chem. **51**, 1221–1230 (2013)
50. F.H. Kaatz, E. Estrada, A. Bultheel, N. Sharrock, Phys. A **391**, 2957–2963 (2012)